CHAPTER 3

MODELLING OF RF PULSE SHORTENING CAUSES AND THEIR EFFECTS ON AN RBWO UNDER LOW GUIDING MAGNETIC FIELD

CONTENTS

*Part of this work has been published as:

V. Venkata Reddy, Mumtaz Ali Ansari and M.Thottappan, "Modeling of RF Pulse Shortening Causes and Their Effects on an Overmoded RBWO under Low Guiding Magnetic Field," ***IEEE Transactions on Electron Devices***, vol. 69, no. 1, pp. 333-339, Jan. 2022 (10.1109/TED.2021.3130860).

Chapter 3: Modelling of RF Pulse Shortening causes and Their Effects on RBWO under Low Guiding Magnetic Field

3.1 Introduction

RBWO is one of the promising HPM devices highlighted at Giga-Watt power level. In microwave technology, the diameter of the device depends on the operating frequency, and both weight and volume depend on the external guiding magnetic field. The need for a strong external guiding magnetic field makes the device bulky, therefore reducing the weight and volume of HPM devices using permanent magnets is beneficial and attractive. The permanent magnets are favorable if the value of guiding magnetic field is less than 1 T, which reduces the system size and energy consumption. The overmoded slow wave structure (OSWS) and trapezoidal resonant reflector (TRR) are used to enable the device to operate in a low guiding magnetic field and high-power generation [83, 96]. The RBWO is more favorable while using OSWS and TRR in view of high-power handling capability, low electric field (E-field) inside the SWS and the surface of reflector to reduce the breakdown problem up to some extent, large space charge limiting current, and OSWS also facilitate the increase in span for the operating guiding magnetic field to overcome cyclotron absorption at the lower guiding magnetic field [125]. However, the problem of mode competition is likely to be found in OSWS. Therefore, the desired mode selection methods and mode purity techniques [128] are needed to improve the device performance. TRR improves the reflection coefficient and bandwidth for the desired mode of operation and enhances frequency tuning [63]. The momentum spread is also low, which is beneficial for high efficiency [8, 96]. The above methods are combined with low guiding magnetic field operation in RBWO design to reduce the pulse shortening.

In the past few decades, many researchers have studied RBWOs at low guiding magnetic fields (i.e., < 1 T). Kurkan *et al*. [6] have experimentally tested an overmoded RBWO at low guiding magnetic field of ~0.7 T, with pulse width ~10 ns. An overmoded slow-wave HPM generator experimentally demonstrated at ~0.6 T, with a efficiency of ~21 % [129]. Totmeninov *et al*. [130] have experimentally studied an RBWO operated in repetitively pulsed mode under ~0.4 T, with pulse width of ~20 ns. Zhang et al. [131] experimented with an X-band RBWO at ~0.7 T, with ~30 % efficiency. A rectangularly corrugated overmoded RBWO using RR was designed and simulated under ~0.48 T, with ~30 ns pulse at ~12.3 GHz [132]. Li *et al*. [133] have designed and simulated an RBWO using a rectangular reflector, modulation cavity, and dual cavity extractor with a single mode structure under ~0.88 T, with ~37 % efficiency. In parallel, a high efficiency RBWO using a TRR, modulation cavity, and dual cavity extractor was also examined under ~0.95 T using particle-in-cell (PIC) technique [8]. More recently, Ansari *et al.* [134] have designed and studied an X-band non-uniform RBWO using TRR under ~0.57 T for ~100 ns without any pulse shortening.

In the chapter, four different configurations of S-band RBWO with the non-overmoded / overmoded SWSs and RR / TRR are investigated for the RF pulse shortening studies at low guiding magnetic field. The work is also intended to mitigate the problem of RF pulse shortening. In Section 3.3, the design and simulation of non-overmoded RBWO with RR presented for the preliminary investigation on the saturated RF output power and power duration at low guiding magnetic field.

3.2 Overview of Simulation Techniques in VED's

Manufacturing issues, design, analysis and cost are the main concern for the design and development of VEDs and HPM systems. Simulation techniques make things possible to design and optimized the parameters before going for experimental studies and

reduce the investment cost. Researchers are using various kinds of simulation tools that employ various techniques from last couple of decades, since then great advancements have been done in the era of EM simulations techniques. Now-a-days, various simulation tools are commercially available such as MAGIC-3D, CST Microwave Studio, KARAT, HFSS, etc. [135]-[138], which are more precise, consistent, flexible and user-friendly. 3D simulation provides the virtual environment to study the various parameters related to VEDs such as design and development of device, mode of propagation, field calculations, and beam-wave interaction. 3D simulations can check the operational limits of the device and examine the unfavorable effects on the operation of the device in the range of predicted parameters. The above advantages suggested that EM simulation tools should be included as an integral part of design and development study of HPM devices.

The wave equations and particle dynamics have been calculated using different Numerical techniques, which are classified based on the surface or volume integral and differential equation methods [139]. The volume and surface integral methods lag with time complexity and not suitable for complex problems. Thus, differential equation-based methods such as Finite Element Method (FEM), Finite Difference Time Domain (FDTD), and Finite Integration Technique (FIT) are being used extensively, as it reduces the complexity by separating the solution space to the wave equations. The FEM is a frequency domain based numerical technique, which divides the space into sub-elements such as Triangles (2D) and Tetrahedral (3D), whereas the FDTD comprises of spatial and temporal variation of the curl equations by using YEE's cell. The FDTD is an accurate and fast numerical technique for computing structured Cartesian grids. The FIT converts Maxwell's integral equations into set of linear

equations. The interface between different media, curved boundaries and complex structures are commutated without degradation of accuracy.

The 3D simulation studies of the RF interaction structure for VEDs have divided into two stages: Beam absent study referred to as Cold Simulation and beam present study referred as Hot Simulation. CST Microwave Studio, HFSS and COMSOL are commercially available 3D simulation software based on FIT or FEM and are commonly being used for cold simulations. Among them, the CST Microwave Studio simulation tool is being widely used because of large and versatile problem-solving approach and it consists of seven solvers for a vast range of EM problems in different structures [136]. While for Hot simulations, CST PS and MAGIC 3D are the popular simulation tools. These simulation tools are being used to study the beam-wave interaction mechanism using particle-in-cell (PIC) technique [135-137]. KARAT and MAGIC-3D PIC simulation are based on different variant of FDTD techniques. Among all MAGIC-3D is being widely used PIC solver for beam-wave interaction studies of VEDs sources because of its accuracy.

3.3 Design and Simulation of Non-Overmoded RBWO with RR

2D modeled structure in the cylindrical coordinate system [Figure 3.1] of an S-band RBWO that includes an explosive emission cathode, a cavity RR, a drift section followed by non-overmoded SWS, and a tapered collector. The design parameters of the present RBWO structure are given in Table 3.1. The mean diameter ($D = 2r_0$) of SWS is chosen ~1.17 times the free space wavelength (λ). The emitted annular IREB is passed through the RR, SWS for beam modulation and interaction with the RF signal and finally collected at the tapered collector. There are two resonance magnetic fields for cyclotron absorption of generated power [125] in RBWO, which are calculated using equations (2.21) and (2.22), respectively.

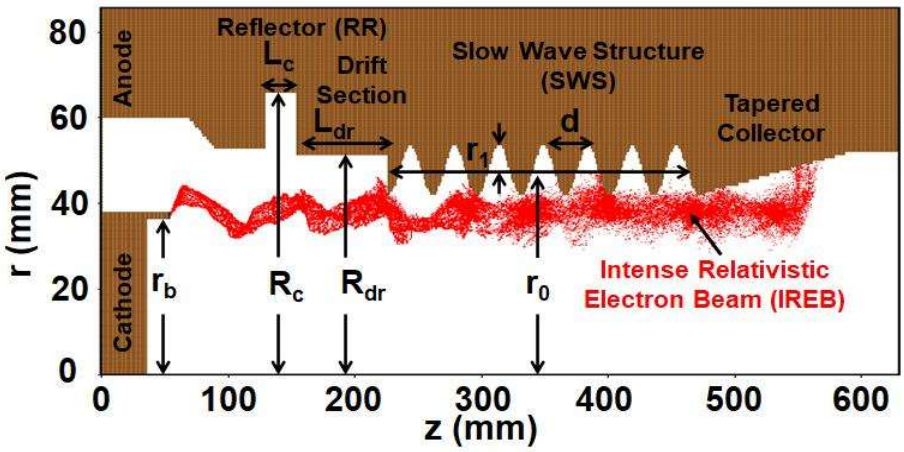

Figure 3.1: 2D Model simulation structure of non-overmoded RBWO (D/λ ≈ 1.17) with RR under guiding magnetic field ~0.22 T and DC input voltage 550 kV.

In the present design, the corresponding cyclotron resonance absorption magnetic field values B_1 and B_2 are calculated as ~0.10 T and ~0.57 T [Figure 3.2], respectively. The PIC simulation of the present RBWO predicted an RF output power of ~0.96 GW under ~0.22 T with DC input voltage 550 kV and developed current ~5.9 kA. The obtained RF output power is without consideration of the causes of the RF pulse shortening. However, the power duration is ~20 ns, and saturated RF output power is shortened after ~36 ns [Figure 3.3 (a)] due to the smaller diameter of the SWS and RR. The frequency spectrum [Figure 3.3 (b)] of the generated microwave shows that the device operates at ~3.7 GHz without any higher harmonics and mode competition.

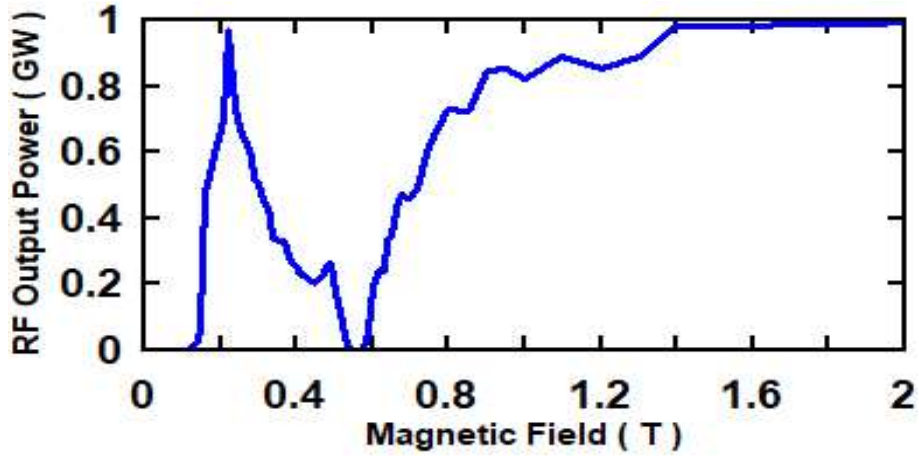

Figure 3.2: RF output power versus magnetic field for non-overmoded RBWO (D/λ ≈ 1.17) for the DC input voltage 550 kV. The cyclotron resonances magnetic fields are found at B1 ≈ 0.10 T and B2 ≈ 0.57 T.

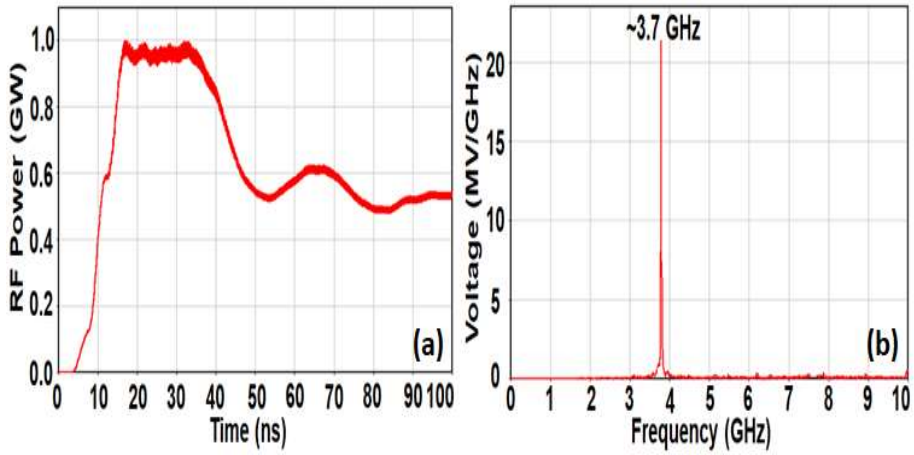

Figure 3.3: (a) RF output power and (b) FFT of the RF output signal of non-overmoded RBWO (D/λ ≈ 1.52) with RR under guiding magnetic field of ~0.22 T.

Table 3.1: Design Parameters for the four configurations of RBWOs

Parameter		**Values (D/λ≈1.17)**	**Values (D/λ≈1.52)**
Non-Overmoded RBWO with RR and Overmoded RBWO with RR			
Slow Wave Structure (SWS)	Mean radius (r_o)	47.98 mm	62.53 mm
	Ripple amplitude (r_1)	05.81 mm	05.89 mm
	Period (d)	34.99 mm	34.40 mm
	SWS length (N)	7*d mm	7*d
Rectangular Resonant Reflector (RR) and Drift Section	Reflector length (L_c)	25.00 mm	25.00 mm
	Reflector radius (R_c)	66.00 mm	76.55 mm
	Drift length (L_{dr})	72.5 mm	78.8 mm
	Drift radius (R_{dr})	51.80 mm	67.00 mm
Non-Overmoded RBWO with TRR and Overmoded RBWO with TRR			
Slow Wave Structure (SWS)	Mean radius (r_o)	47.98 mm	62.53 mm
	Ripple amplitude (r_1)	05.81 mm	05.89 mm
	Period (d)	34.99 mm	34.40 mm
	SWS length (N)	7*d	7*d
Trapezoidal Resonant Reflector (TRR) and Drift Section	Reflector length (L_c)	40.75 mm	40.75 mm
	Reflector radius (R_c)	66.00 mm	78.57 mm
	Drift length (L_{dr})	75.50 mm	79.8 mm
	Drift radius (R_{dr})	51.80 mm	67.00 mm

To further improve the overall performance of the device in terms of saturated RF output power without any pulse shortening, another three different configurations of RBWOs are simulated. The causes of RF pulse shortening environment are also coded in MAGIC-PIC simulation to analyze effects over four configurations. The design parameters of the four configurations (non-overmoded RBWO with RR, non-overmoded RBWO with TRR, overmoded RBWO with RR, and overmoded RBWO with TRR) are listed in Table 3.1. The overmoded RBWO is obtained by replacing non-overmoded SWS with overmoded SWS ($D/\lambda \approx 1.52$). The overmoded SWS has reduced the magnetic field from ~0.22 T to ~0.19 T (Figure 3.4), as compared to non-overmoded SWS (Figure 3.2), and the cyclotron resonance absorption [125] magnetic fields are calculated for the overmoded case as, ~0.07 T and ~0.49 T. The same values are observed with simulation also, as shown in Figure 3.4. Next, the TRR is designed so that the sidewalls of the RR are sloping outward, as shown in Figure 3.5, and the length of the TRR is Lc1 = Lc2 = Lc3 = Lc /3. The design parameters given in Table 3.1 are optimized for a high saturated RF output power and longer power duration for each configuration. The dispersion diagram of non-overmoded RBWO with RR and TRR and overmoded RBWO with RR and TRR is shown in Figure 3.6. It is observed that the beam mode line with a beam voltage of 550 kV intersects with -1st harmonics of the waveguide mode line (i.e., TM_{01}) at ~3.7 GHz of non-overmoded SWS and OSWS. The DC input power drives the four combinations of RBWO's ~3.25 GW (550 kV * 5.9 kA) and developed a current of ~5.9 kA for 100 ns with the rise time of 1 ns, as observed in Figure 3.7. The modelling of various causes of RF pulse shortening and the effect of causes of pulse shortening on each configuration and its simulation results are discussed in section.

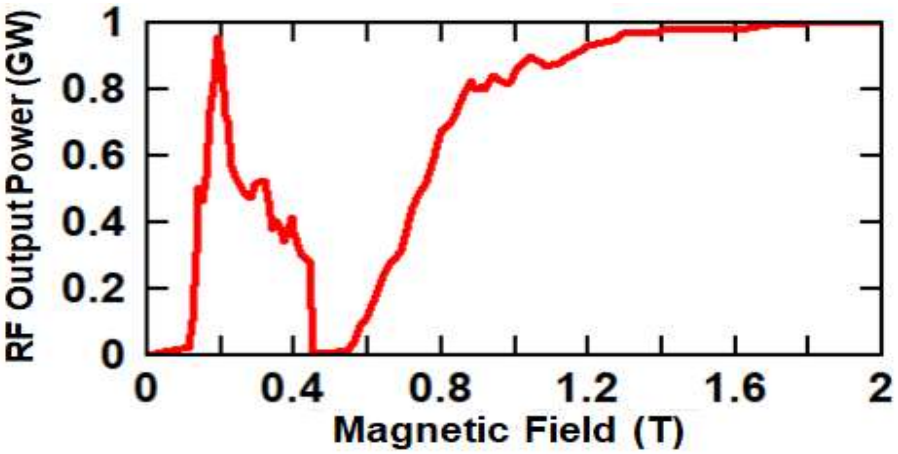

Figure 3.4: RF output power versus magnetic field for overmoded RBWO ($D/\lambda \approx 1.52$) for the DC input voltage 550 kV. The cyclotron resonances magnetic fields are found at $B1 \approx 0.07$ T and $B2 \approx 0.49$ T.

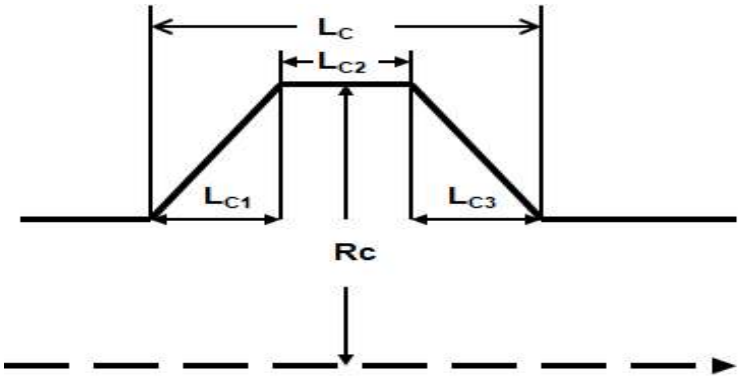

Figure 3.5: 2D The Schematic of Trapezoidal Resonant Reflector (TRR).

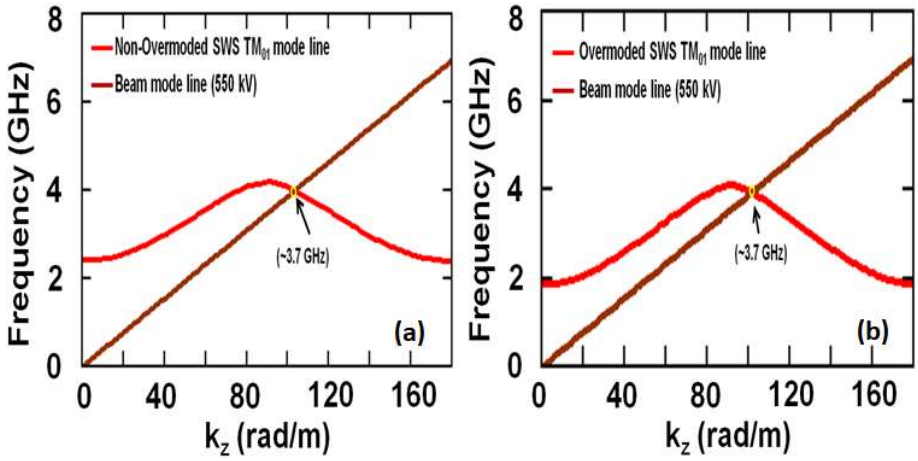

Figure 3.6: Dispersion curve for (a) non-overmoded RBWO and (b) overmoded RBWO showing TM_{01} mode line and beam mode line intersecting at ~3.7 GHz.

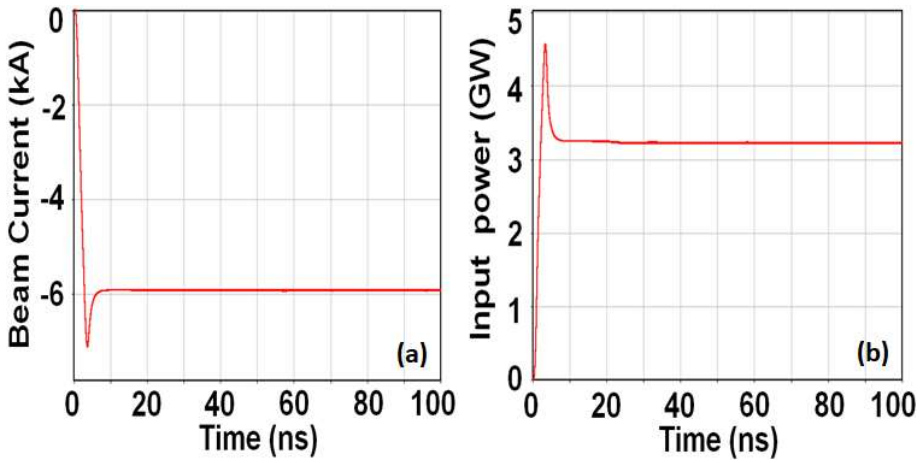

Figure 3.7: (a) Developed electron beam current ~5.9 kA, and (b) DC beam power (voltage*current) ~3.25 GW when the applied beam voltage is 550 kV.

3.4 Simulation Study of RF Pulse Shortening

3.4.1 Modeling of various causes of RF pulse shortening

In HPM devices, the various causes of RF pulse shortening are: (i) beam disruption, (ii) secondary electron emission (SEE), (iii) high electric field electron emission (HEE), and (iv) plasma ions generation at the collector wall [107]. The modeling of various causes of RF pulse shortening using 3D electromagnetic "MAGIC" code is discussed in the following sections.

Cause 1: Beam Disruption: - The beam quality is deteriorated due to the smaller diameter of the device and low guiding magnetic field. The thickness of the annular beam expands/grows in the transverse direction at the end of SWS [Figure 3.8], which leads to the mitigation of beam-wave coupling and can cause non-linear instabilities such as cross excitation and suppressing the RF output power generation [107]. The expanded annular electron beam is intercepted with SWS, which can increase the gap closure problems and causes the beam termination. PHASE SPACE AXES X_2 P_2 command is used to observe the expanded beam inside the device (P_2 is axial momentum and X_2 is radial coordinate), which plots the radial momentum of the beam

Figure 3.8]. Using these plots, the amount of expansion of beam thickness in the radial direction is estimated.

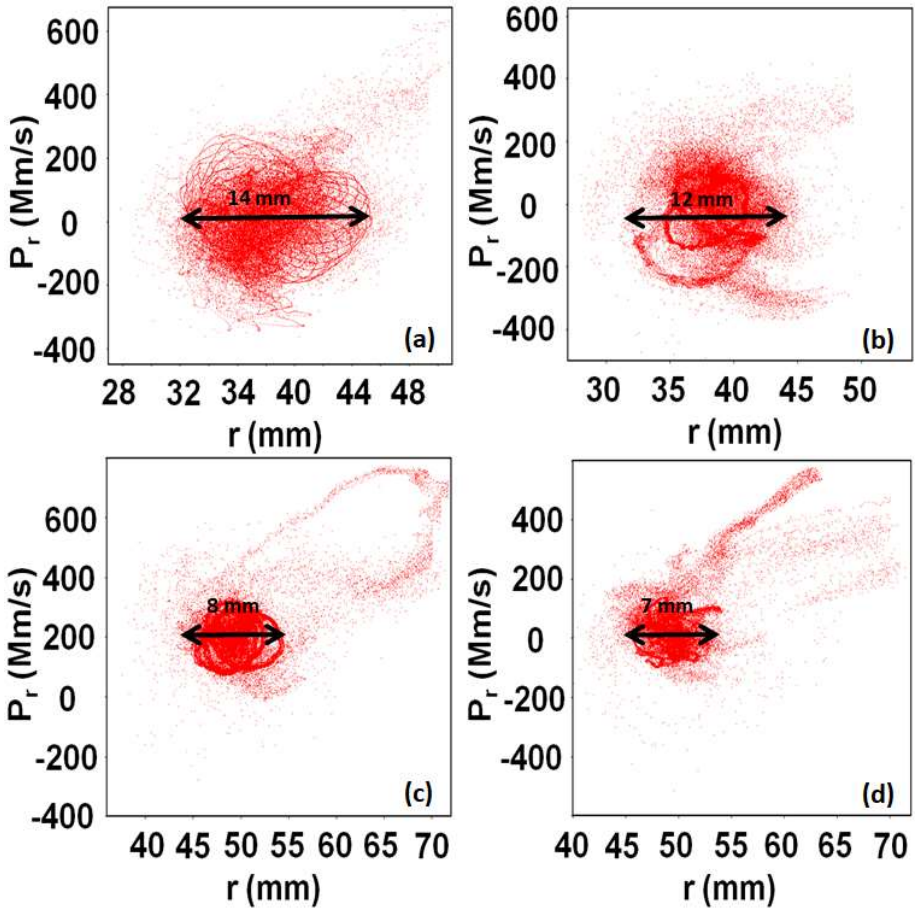

Figure 3.8: Phase space plot of traversed electrons (at the end of SWS) in radial momentum at ~100 ns in (a) non-overmoded RBWO ($D/\lambda \approx 1.17$) with RR at B= ~0.22 T, (b) non-overmoded RBWO with TRR B= ~0.22 T, (c) overmoded RBWO ($D/\lambda \approx 1.52$) with RR at B= ~0.19 T, and (d) overmoded RBWO with TRR at B = ~0.19 T.

Cause 2: Secondary Electron Emission (SEE): - It is the phenomenon by which the primary electrons strike the inner surface of the device with sufficient energy and let other electrons to come out of the surface, *i.e.*, secondary electrons [secondary electrons due to SEE in Figure 3.9]. These electrons suppress the RF output power with a self-generated oscillating space charge due to multipactor effect. To evaluate the effectiveness of SEE, EMISSION SECONDARY command is used, which enables the release of secondary electrons from the surface of the conducting spatial object, as they are affected by primary particles. The energy of the primary electrons hitting the surface

of the structure at the dump location after the interaction is measured as ~420 keV. The yield value (ratio of secondary electrons to incident electrons) is calculated as ~0.8.

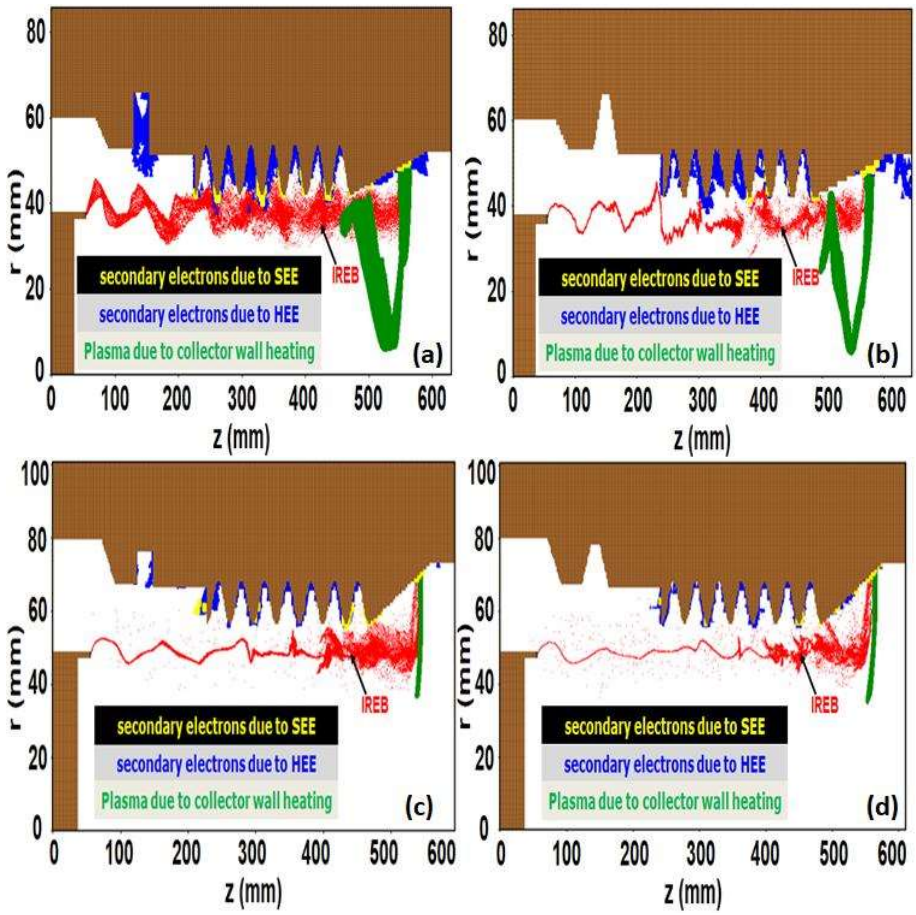

Figure 3.9: Phase space plot distribution showing combined influences of SEE (yellow color), HEE (blue color), PCHI (green color) at ~100 ns in (a) non-overmoded RBWO ($D/\lambda \approx 1.17$) with RR at B= ~0.22 T, (b) non-overmoded RBWO with TRR at B= ~0.22 T, (c) overmoded RBWO with ($D/\lambda \approx 1.52$) RR at B= ~0.19 T, and (d) overmoded RBWO with TRR at B= ~0.19 T.

Cause 3: High Electric Field Electron Emission (HEE): - The strength of the RF electric field (E-field) developed inside the microwave device is another source of electron emission [secondary electrons due to HEE in Figure 3.9]. The high electric field triggers the explosive emission from inner surface of the reflector and SWS, which causes the surface breakdown [106]. The developed high electric field inside the device also resonates with the operating frequency and can absorb the power from generated microwave. This leads to the partial termination of the generated microwave. The HEE

is measured by using the EMISSION EXPLOSIVE THRESHOLD command. The breakdown can occur only if the developed RF electric field exceeds the threshold value. The CONTOUR FIELD E1 command measures the electric field's strength in the beam present condition for causing the pulse shortening. It is used to plot the contours of electromagnetic field variables over a specified two-dimensional spatial region.

Cause 4: Generation of Plasma Ions at Collector Wall: - The limitation of saturated RF output power and its power duration in most HPM devices is due to the desorption of gases, atoms, and oil molecules from the inner surface of the metal. Water molecules and other gases are desorbed from the beam dump position at the collector surface and disassociated into positively charged hydrogen ions (PCHI) and other light elements [140, 141]. The PCHI are considered in the present pulse shortening study, as it is the lightest and fastest one. The dense PCHI absorb energy from the generated microwave power and suppress the generation [142]. The formation of PCHI at the inner surface of the metal collector is observed by using EMISSION EXPLOSIVE WALL_TEMPERATURE (Temp, z) command. The command allows specifying the generation of PCHI. It depends on temperature and position of collector wall, where the beam hits the surface of the collector wall specifically chosen. A ~45 mm axial variation of the collector surface is chosen to measure the temperature at which the beam is dumped at the inner surface of the collector. The PCHI is evaluated using the temperature and position at the conducting wall. The initial ambient temperature is 293 K, which increases as the charged particles deposit the energy on the surface of the structure. Desorption of gas molecules is significant when the wall temperature rises from the absolute room temperature (i.e., 300 K). The collector wall temperature can increase by ~100 ^{0}C in 100 ns if the current density is ~100 A /cm^{2} and in ~10 ns if the current density ~1000 A /cm^{2} [143]. Also, the primary electrons with an energy of

around 100 keV can desorb at least 1 molecule from the wall wherever striking [144]. In the present case, the primary electrons with the energy >100 keV (~420 keV) after the interaction striking continuously at the beam dump location can cause large molecules' desorption. In overmoded RBWO, the current density is lower than in non- overmoded RBWO because the beam radius is larger than that in overmoded RBWO.

The temperature rise is based on the current density developed in the device. The temperature rise is measured at the beam dumped location as shown in Figure 3.10. As the wall temperature increased beyond the absolute room temperature, the atoms and gaseous molecules are desorbed from the beam dump position at the collector and ionized by the primary IREB or secondary electrons. The resulting PCHI [PCHI due to collector wall heating in Figure 3.9] moves toward the interaction region with the external guiding magnetic field's influence. The generated PCHI severely affects the RF pulse shortening.

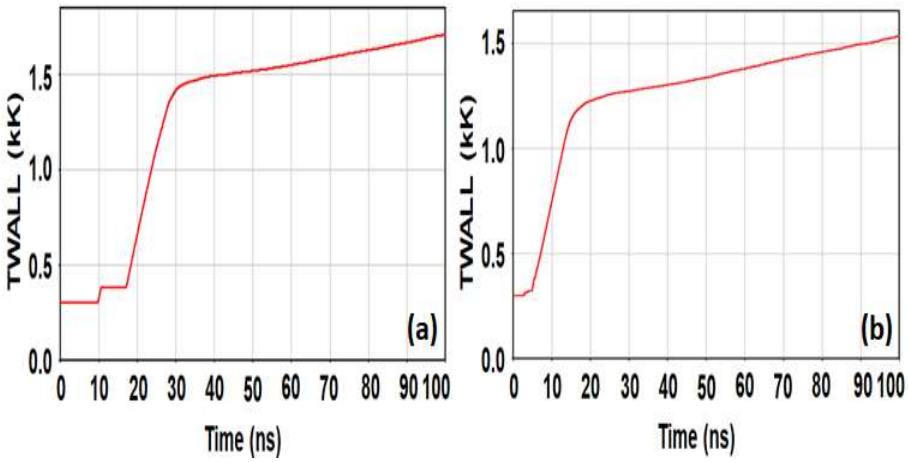

Figure 3.10: Variation of temperature at the collector conducting wall w.r.t to time for (a) non-overmoded SWS, and (b) overmoded SWS.

3.4.2 Simulation Study of Combined Causes of RF Pulse Shortening and their effects in RBWO Operation

The above RF pulse shortening causes are combined to analyze their effects over the microwave generation in both non-overmoded and overmoded RBWO with RR and TRR combinations.

Case 1: Non-Overmoded RBWO with RR: **-** The effect of beam degradation in RBWO is severe due to the low guiding magnetic field and the development of a high RF electric field for the smaller diameter of SWS. The amount of beam expansion in radial momentum [Figure 3.8 (a)] shows that the beam has gained the radial momentum and the beam thickness expanded from 2 mm (beam at the cathode) to 14 mm (beam at the end of SWS). The degraded beam causes non-linear instabilities and ultimately results in the suppression of saturated RF output power. The low guiding magnetic field (~0.22 T) and high E-field strength of ~730 kV/cm in the reflector and ~790 kV/cm in SWS [Figure 3.11], which stimulate the degradation of electron beam and hence the SEE (yellow color) and HEE (blue color), respectively [Figure 3.9 (a)]. Due to the continuous bombardment of the electron beam at the collector surface, the collector wall temperature is increased rapidly in the non-overmoded RBWO [Figure 3.10 (a)]. With this, the PCHI has begun to originate from the collector wall and travelled towards the RF interaction region area under the guidance of a static electric field generated by the IREB and an external magnetic field (~0.22 T) [Figure 3.9 (a)] to limit the IREB transmission. In this process, the IREB's space charge potential provides kinetic energy to PCHI. The moving PCHI can degrade the beam-wave coupling and shorten the electron beam with the inner surface of the conductor [107, 142]. Therefore, the combined effect of these causes of RF pulse shortening has highly suppressed the microwave generation, as shown in Figure 3.15 (brown color curve) [145]. The

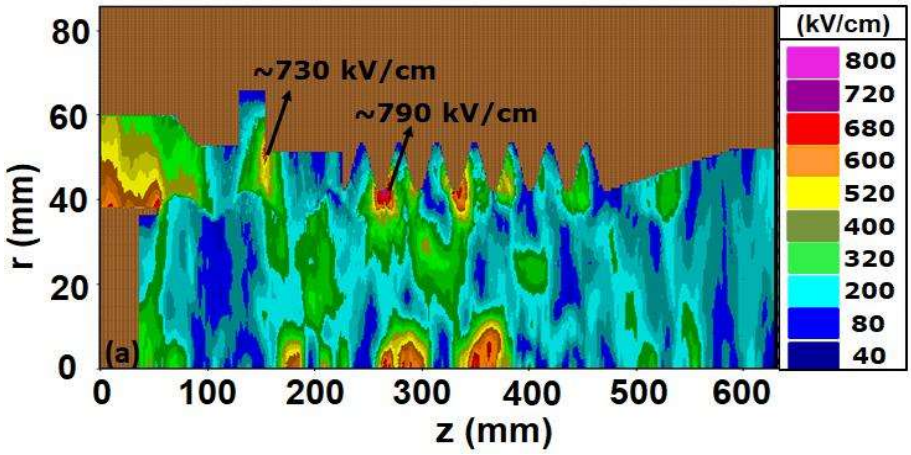

Figure 3.11: Contour plot of the RF electric field at ~100 ns in non-overmoded RBWO (D/λ ≈ 1.17) with RR under the guiding magnetic field ~0.22 T.

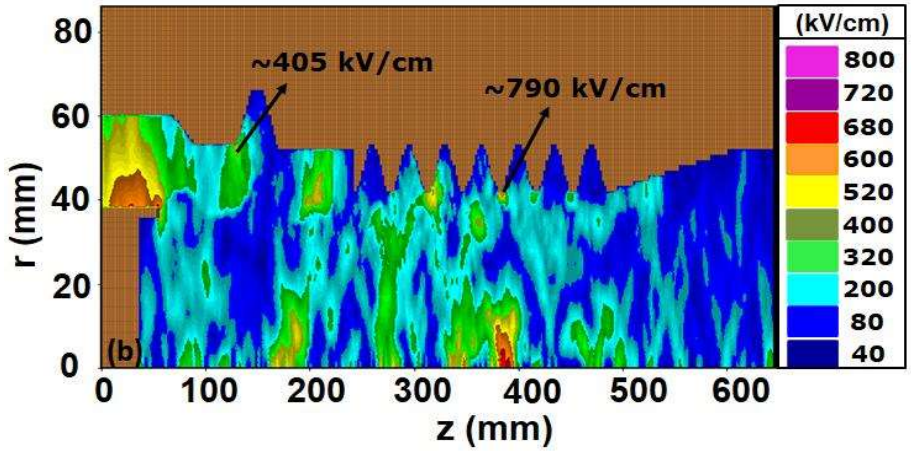

Figure 3.12: Contour plot of the RF electric field at ~100 ns in non-overmoded RBWO (D/λ ≈ 1.17) with TRR under the guiding magnetic field ~0.22 T.

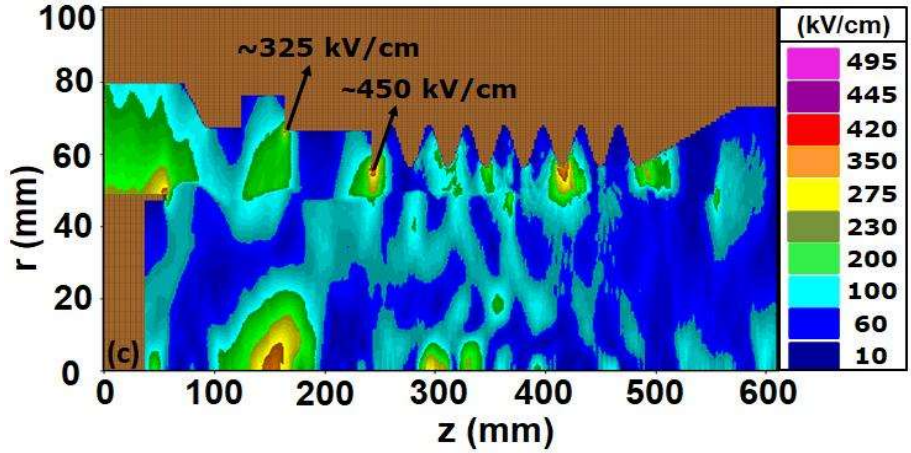

Figure 3.13: Contour plot of the RF electric field at ~100 ns in an overmoded RBWO (D/λ ≈ 1.52) with RR under the guiding magnetic field ~0.19 T.

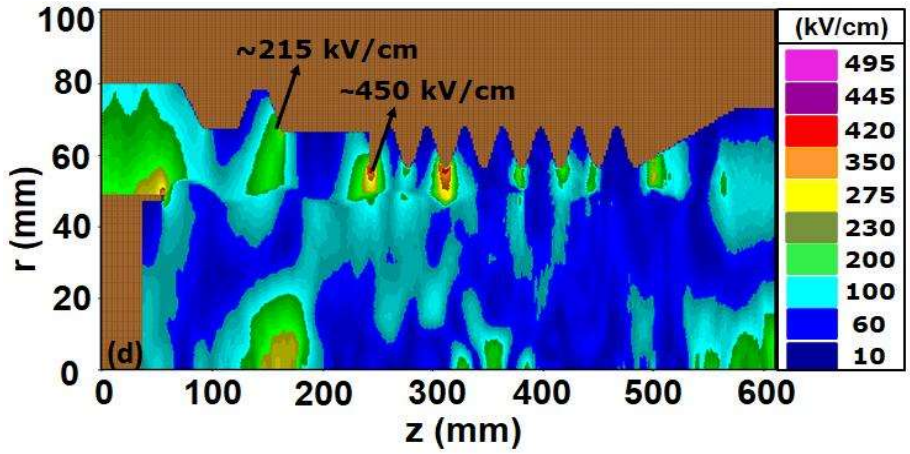

Figure 3.14: Contour plot of the RF electric field at ~100 ns in an overmoded RBWO (D/λ ≈ 1.52) with TRR under the guiding magnetic field ~0.19 T.

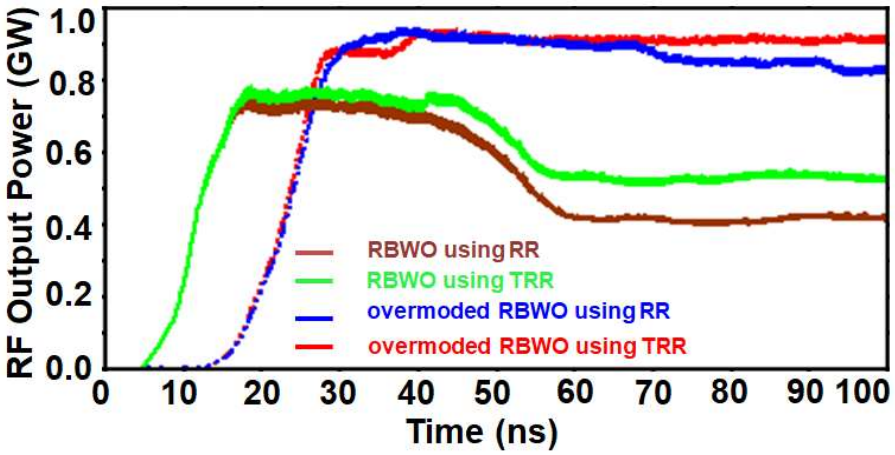

Figure 3.15: RF output power for all four configurations of RBWOs after including the combined causes of pulse shortening.

generated saturated RF output power is only ~0.75 GW, and the power duration is limited to ~15 ns. The saturated RF output power begins to decrease after the simulation time ~30 ns.

Case 2: Non-Overmoded RBWO with TRR: - The effect of beam expansion in radial momentum [Figure 3.8 (b)] shows that the beam thickness reduced from 14 mm to 12 mm due to the introduction of TRR in the non-overmoded RBWO configuration as compared to non-overmoded RBWO with RR [Figure 3.8 (a)]. The TRR reduced the E-field strength around the reflector's edges from ~730 kV/cm (Figure 3.11 for RR) to

~405 kV/cm (Figure 3.12 for TRR). The reduced E-field has improved the quality of the electron beam at the reflector [electron beam at the reflector in Figure 3.9 (b)] and reduced the emission of electrons from the explosive emission centers at the reflector (blue color). The reduction of electron emissions due to HEE enhanced the generation efficiency and duration of the saturated RF output power. The present non-overmoded RBWO with TRR has generated a saturated RF output power of ~0.79 GW with improved power duration up to ~30 ns (green color line in Figure 3.15), as compared to the non- overmoded RBWO with RR. The guiding magnetic field remains the same i.e., ~0.22 T, which means that the introduction of TRR in non-overmoded RBWO has improved the device performance by enhancing the power duration.

Case 3: Overmoded RBWO with RR: - To further improve the device generation efficiency and power duration, an overmoded SWS ($D/\lambda \approx 1.52$) is used with RR. The overmoded SWS reduces the beam degradation even at a low guiding magnetic field (~0.19 T) and improves the quality of the electron beam [electron beam in Figure 3.9 (c)]. It can be seen from the transverse variation of radial momentum in Figure 3.8 (c), which shows that the beam thickness is started with 2 mm and expanded up to 8 mm. The expansion of beam thickness is decreased in overmoded SWS with RR [8 mm in Figure 3.8 (c)], as compared to non-overmoded SWS with TRR [12 mm in Figure 3.8 (b)]. The strength of the electric field in beam present condition is measured as ~325 kV/cm (reflector) and ~450 kV/cm (SWS) [Figure 3.13], which is even less than the fields measured in RR (~730 kV /cm), in TRR (~405 kV /cm) and SWS (~790 kV/cm) in the previous two configurations, as shown in Figure 3.11 and Figure 3.12, respectively. The use of overmoded SWS has minimized the amount of beam degradation, and E-field concentrated around the inner surface of the SWS. Very few electrons (yellow and blue colors in Figure 3.9 (c)) other than the primary electrons

emitted, as compared to non-overmoded RBWO (Figure 3.9 (a) and Figure 3.9 (b)) irrespective of the reflector. Furthermore, the collector plasma generation at the overmoded SWS-collector surface has significantly delayed [Figure 3.9 (c)] due to the wall temperature increases slowly [Figure 3.10 (b)], while in non-overmoded SWS-collector wall surface temperature increases rapidly [Figure 3.10 (a)]. The collector wall of the overmoded RBWO has a larger surface area, therefore the current density is decreased and limited the temperature rise further and the expansion of collector plasma along with the external guiding magnetic field also decreased. Hence, the RBWO configuration with overmoded SWS and RR has significantly improved the saturated RF output power to ~0.96 GW for ~43 ns of power duration (blue color in Figure 3.15). The larger diameter of the overmoded SWS has reduced the magnetic field from ~0.22 T to ~0.19 T.

Case 4: Overmoded RBWO with TRR: - Finally, the RBWO configuration with overmoded SWS ($D/\lambda \approx 1.52$) and TRR is examined to enhance its overall performance in terms of efficiency and power duration by overcoming the problem of RF pulse shortening associated with the non-overmoded RBWO with both RR and TRR and overmoded RBWO with RR. The effect of beam expansion in radial momentum is shown in Figure 3.8 (d). The beam thickness [Figure 3.8 (d)] is slightly reduced from 8 mm to 7 mm due to the introduction of TRR in the overmoded RBWO configuration, as compared to overmoded RBWO with RR [Figure 3.8 (c)] [Figure 3.8 (c)]. The RF E-field around the edges and surface of the overmoded TRR and SWS is extremely reduced to ~215 kV /cm and ~450 kV /cm, respectively [Figure 3.14]. The reduced E-field highly overcomes the problem of beam degradation at the low guiding magnetic field operation due to OSWS as shown in Fig. 3.9 (d). It is observed that there is no HEE in the TRR region, the amount of SEE (yellow color) is negligible, and the

generation of collector plasma is also significantly low as explained in Case 3. The combination of the overmoded SWS and TRR has generated a saturated RF output power of ~0.96 GW (red color line in Figure 3.14) without any termination of microwave generation of simulation time with a power duration of at least 70 ns at the lower guiding magnetic field of ~0.19 T.

The combined effects of pulse shortening mechanism on RF output power of all four RBWO configurations are shown in Figure 3.15. It is observed that the simulations of non-overmoded RBWO with RR and TRR and overmoded RBWO with RR have predicted the saturated RF output power of ~0.75 GW, ~0.79 GW, and ~0.96 GW for ~15 ns, ~30 ns, and ~43 ns of power duration, respectively. However, the simulation of RBWO using overmoded SWS and TRR predicted the saturated RF output power of ~0.96 GW for at least 70 ns power duration. The performances of all four configurations of RBWO are listed in Table 3.2. It is observed that the overmoded RBWO with TRR is better than non-overmoded RBWO with RR and TRR and overmoded RBWO with RR. In the present simulation, overmoded RBWO with TRR at $D/\lambda \approx 1.52$ predicted the maximum saturated RF output power without any pulse shortening up to 100 ns of simulation time.

Table 3.2: Output parameters of all four configurations of RBWOs after Pulse shortening Analysis.

Configuration of RBWO	**Parameters**			
	Frequency (GHz)	**Saturated RF output Power (GW)**	**Efficiency (%)**	**power duration (ns)**
Non-Overmoded RBWO with RR	3.74	~0.75	~23	~15
Non-Overmoded RBWO with TRR	3.67	~0.79	~24	~30
Overmoded RBWO with RR	3.66	~0.96	~30	~43
Overmoded RBWO with TRR	3.73	~0.96	~30	~70

3.5 Conclusion

The influence of non-overmoded RBWO and overmoded RBWO using RR and TRR on the power duration and the saturated RF output power for the GW level at low guiding magnetic field have been studied by incorporating some of the practical causes of RF pulse shortening using FDTD based PIC simulation of MAGIC code. The causes of RF pulse shortening have greatly influenced the non-overmoded RBWO with RR and TRR at the low guiding magnetic field. The configuration of overmoded RBWO with RR at a low guiding magnetic field had a little effect on RF pulse shortening over the RF generation. The pulse shortening has been completely absent up to 100 ns of simulation time in the combination of RBWO using overmoded SWS and TRR. They are found to have high power handling capability even in the presence of RF pulse shortening mechanisms. This combination has a large diameter that reduces the beam disruption, secondary electron emission, E-field strength at the surfaces of SWS and reflector, and collector's plasma effect at the low guiding magnetic field. Among all four configurations of RBWO, the simulation of the overmoded RBWO with TRR has predicted a saturated RF output power of ~0.96 GW without any pulse shortening for the entire simulation time having the power duration at least 70 ns at the lowest guiding magnetic field of ~0.19 T. The power conversion efficiency of the overmoded RBWO with TRR has been calculated as ~30 % for the DC input voltage 550 kV and developed electron beam current ~5.9 kA.

The limitations of the present simulation work are the absence of plasma formation in the reflector and SWS region and repetitive mode of operation. However, the effect of SEE and HEE on RF pulse generation has been studied in detail. The pulse duration had also been affected, as the device was tested experimentally under repetitive mode of operation [146]. Another limitation of the simulation environment is that

observing several hundreds of pulses under the repetition mode operation is not possible.

The next part of the work is the design of a high efficiency RBWO with the direct generation of linearly polarized Gaussian like TE_{11} mode using a sectional Bragg structure as a reflector as explained in Chapter 4.